Research on Engineering Structures & Materials
www.jresm.org
Research Group

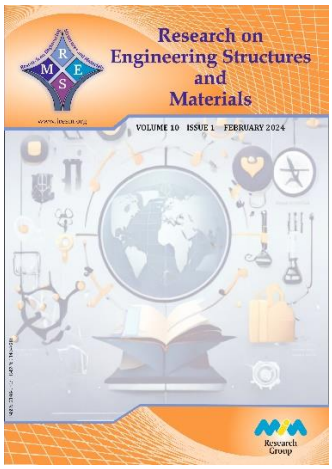

Characterization of thin ITO/Au/ITO sandwich films deposited on glass substrates using DC magnetron sputtering

Tarek Saidani, Mohammed Rasheed, Iqbal Alshalal, Arshad Abdula Rashed, Mohammed Abdelhadi Sarhan, Regis Barille

Online Publication Date: 30 November 2023
URL: http://www.jresm.org/archive/resm2023.21ma0922rs.html
DOI: http://dx.doi.org/10.17515/resm2023.21ma0922rs

Journal Abbreviation: *Res. Eng. Struct. Mater.*

To cite this article
Saidani T, Rasheed M, Alshalal I, Rashed AA, Sarhan MA, Barille R. Characterization of thin ITO/Au/ITO sandwich films deposited on glass substrates using DC magnetron sputtering. *Res. Eng. Struct. Mater.*, 2024; 10(2): 743-770.

Research on Engineering Structures & Materials
www.jresm.org
MIM Research Group

Research Article

Characterization of thin ITO/Au/ITO sandwich films deposited on glass substrates using DC magnetron sputtering

Tarek Saidani[1,a], Mohammed Rasheed[*2,3,b], Iqbal Alshalal[4,c], Arshad Abdula Rashed[5,d], Mohammed Abdelhadi Sarhan[6,e], Regis Barille[3,f]

[1]*Physics of Materials and Optoelectronic Components Laboratory, Faculty of Sciences and Applied Sciences, Akli Mohaned Oulhadj University of Bouira, Bouira, 10000, Algeria*
[2]*Applied Sciences Department, University of Technology- Iraq, Baghdad, Iraq*
[3]*MOLTECH Anjou, Universite d'Angers/UMR CNRS 6200, 2, Bd Lavoisier, 49045 Angers, France*
[4]*Training and Workshops Center, University of Technology- Iraq, Baghdad, Iraq*
[5]*Production Department, Ministry of Oil, Baghdad, Iraq*
[6]*Mathematics Science Department, College of Science, Mustansiriyah University, Baghdad, Iraq*

Article Info

Article history:

Received 22 Sep 2023
Accepted 27 Nov 2023

Keywords:

D.C. magnetron sputtering;
ITO/Au/ITO structure;
Spectrophotometer;
Spectroscopic ellipsometry;
SEM;
AFM

Abstract

The correlation between structural and optical properties of an Au, ITO, and ITO/Au/ITO (IUI), gold, indium tin oxide, and indium tin oxide/gold/indium tin oxide, respectively, sandwich structure thin film has been reported in this study. The deposition of all samples onto glass substrates was carried out using D.C. magnetron sputtering, without the use of substrate heating, and the intermediate layer was a metallic gold film with an 8 nm thickness. The substrate-target distance in the IUI structure was kept constant at 8 nm. X-ray diffraction (XRD), atomic force microscopy (AFM), and scanning electron microscopy (SEM) are often utilized techniques for the evaluation of the structural and surface morphology of films. The optical properties of the films were demonstrated by a spectrophotometer (UV/vis/NIR) and spectroscopic ellipsometry (SE) techniques adopted for the new amorphous model, and the findings were compared with those between 200 and 2200 nm, where the wavelengths overlap at room temperature, which is the purpose of the present work. The observed and estimated optical constant values of the Au, ITO, and IUI films using the best dispersion model were reported. In addition, the transmission and reflection spectrum results of the films were compared with those obtained by UV measurements. Excellent correlations for the optical constant properties of the multilayer films were observed employing two distinct approaches. These thin films have great promises for the future of transparent conductive oxides (TCOs) and even industrial applications.

1. Introduction

Transparent conducting oxides (TCOs) have favorable electrical conductivity that is similar to that of metals and good optical transmission in the visible region. Examples of TCOs that are gallium-doped are zinc oxide (ZnO), tin oxide (SnO_2), aluminum-doped zinc oxide (AZO), gallium-doped zinc oxide (GZO), fluorine-doped tin oxide (FTO), indium tin oxide (ITO), etc. TCOs refer to a class of semiconductors that exhibit both n and p- type conductivity. These materials possess a broad optical bandgap and a significant number of free electrons in the upper conduction band (CB). Due to the unique properties of ITO thin

*Corresponding author: rasheed.mohammed40@yahoo.com
[a] orcid.org/0000-0002-7727-4734; [b] orcid.org/0000-0002-0768-2142; [c] orcid.org/0000-0003-0948-7460; [d] orcid.org/0009-0004-8179-6190; [e] orcid.org/0000-0002-7011-6581; [f] orcid.org/0000-0001-8792-5118
DOI: http://dx.doi.org/10.17515/resm2023.21ma0922rs

films, ITO electrodes made of transparent conducting oxide have a high transmission over the visible spectrum, which is a property of thin films. Wide optical band gap semiconductors with good electrical conductivity have been widely utilized as transparent conductor electrodes for several electronic devices, like organic light-emitting diodes (OLEDs), solar cells, flat panel displays, gas sensors, liquid crystal devices, and touch screens, are often utilized in modern technology [1–7]. In recent years, to coat high-quality ITO thin films, different researchers have investigated the many advantages of using the direct-current magnetron sputtering technique to coat ITO/metal/ITO sandwich structures with Ag or Au interlayers to enhance the structural, surface morphology, and optical characteristics of the films [8]. The major advantages of using this technique are that it is low-cost, the substrate temperature is 300 K, uniform films have been obtained, and the power source is easy to control. As transparent conducting oxide thin films, ITO, FTO, or ZnO:Al (AZO) single-layer thin films formed on glass substrates have been the most common kind utilized up to this point. In recent years, the requirement for and application of TCOs with great performance have increased continuously. At the moment, ITO and fluorine tin oxide (FTO) seem to be the most promising commercial materials for transparent electrodes. There are a large number of researchers advancing the properties of TCO thin films and amended materials [9–11]. Yet, because of its scarcity on Earth and its high price, indium is not widely utilized, leading the research community to look for other materials with equivalent quantities in terms of electrical and optical characteristics. ITO thin films typically vary in thickness from 150 nm to 700 nm when utilized as a topic of interest is to the transparent electrodes (TCs) associated with optoelectronic devices. The decreasing in film's thickness below 150 nm leads to a significant increase in electrical resistance due to the well-known size effect. Oxide, metal, and oxide films have properties that are mightily dependent on the intermediate layer [12]. Using sandwich structures made of oxide, metal, and oxide to create transparent electrodes has various benefits.

One benefit of using ITO is that the amount of indium is reduced by reducing the thickness of the films' thickness from 150 nm to a total of 50–60 nm for both oxide layers. If we consider the topic of electrical conductivity simultaneously, the optical quantities of the electrode are absolutely preserved and even enhanced. Many studies prove that this type of thin film has very good mechanical properties for wide-scale implementation [13–17]. Until now, researchers have been searching for a substitute for transparent conductive thin films for the alternation of ITO through various experimental tests. Spectroscopic ellipsometry is an indirect, very accurate, non-destructive, non-invasive, non-contact, and very sensitive method for studying single- and multi-layer films. SE gives a method that anyone can use to figure out the exact optical constants and electrical transport properties of single and sandwich films [18–25]. Spectroscopic ellipsometry (SE) is an optical metrology technique that is both non-destructive and non-intrusive, providing surface sensitivity. It involves measuring the change in the polarization state of light when it is reflected at an oblique angle from a thin-film sample. It is frequently used to examine the thickness and optical constants of single- and multilayer thin films [26-30]. A variety of thin film applications, including semiconductors, solar, optoelectronics, optical and functional coatings, surface chemistry, and biotechnology, can be achieved using spectroscopic ellipsometry in conjunction with the robust and user-friendly DeltaPsi2 software, accessories, and equipment [31-57].

The ITO/Au/ITO (IUI) multilayer structure thin film studied in this paper was made by direct-current magnetron sputtering using Au as the intermediate thin film on a glass substrate. The optical properties of each layer in the sandwich structure were studied using UV spectrophotometer and spectroscopic ellipsometry in the same wavelength region for each technique. This methodology enables a more precise determination of the optimal dispersion formula for each individual layer.

2. Experimental Details

A direct-current sputtering process was utilized to prepare (IUI) ultra-thin films on glass substrates without any heating. These materials were deposited in a reactive atmosphere utilizing In:Sn (purity: 90, 10)% and gold (purity: 99.95%) targets, respectively. The gold-intermediated thin film was deposited in an argon atmosphere. Glass slides, 75–50 mm in diameter, from TED PELLA INC. were cut into 2.5–2 cm plates with a thickness of 1.1 mm and utilized as substrates in the present work. Glass plates were cleaned carefully in an ultrasonic bath treatment type (BRANSON Ultrasonic-CAMDA 19 SPC) with ethanol, acetone, deionized water, and finally dichloromethane. Each solution was kept for 20 minutes and dried with a nitrogen gas jet. Then, the glass substrate was placed in a vertical shape according to the target substrate configuration onto a rotating disk kept at ambient temperature. The distance between the target and substrate was kept at about 70 mm, and the parameters of the deposition of Au, ITO, and IUI thin films are presented in Table 1. These parameters are similarly used in the literature pointed in this table.

The target-to-substrate distance was (70 mm) in many reasons:

- The target-to-substrate distance plays a critical role in sputtering processes. A longer distance can result in a more focused deposition area, whereas a shorter distance can lead to a broader deposition area.
- In this case, a target-to-substrate distance of 70 mm may have been chosen for several reasons:
    - Adequate Coverage: A longer distance can help ensure that the sputtered particles have a relatively uniform distribution over the glass substrate, covering a larger area.
    - Minimizing Backscattering: Longer distances can reduce the likelihood of backscattered particles from the target reaching the substrate, which can lead to contamination or inconsistent film properties.
    - Specific Film Thickness: Depending on the desired film thickness, the distance might be adjusted to achieve the target thickness effectively.

2.1. Deposition Current (0.3 A)

- Deposition current controls the sputtering rate. The higher the current, the faster the deposition rate.
- Selection of a deposition current of 0.3 A may be based on the desired film growth rate, the target material's sputtering characteristics, and power supply limitations.
- Justification:
    - Film Thickness Control: A lower deposition current allows for more precise control over film thickness, which is essential when aiming to create ultra-thin films.
    - Reduced Heat Generation: Lower current can also help minimize heat generation during the sputtering process, which aligns with the statement that no heating was applied.
    - Target Material Compatibility: The deposition current should be set within the limits that ensure efficient sputtering of the target material without overheating or damaging it.

2.2 Pressure Variation

- Pressure within the sputtering chamber affects the sputtering process in various ways.
- In the absence of specific information, the pressure may have been varied for the following reasons:
  - Sputtering Rate: Pressure can influence the sputtering rate. Higher pressures can increase the sputtering rate, while lower pressures might yield slower rates.
  - Film Density and Structure: Pressure can impact the density and structure of the deposited film. Higher pressures can result in denser films, while lower pressures may lead to more porous films.
  - Target Erosion and Deposition Uniformity: Pressure can affect the erosion rate of the target material and the uniformity of film deposition.

Without specific details about the pressure variations used, it's challenging to provide a precise explanation or justification. Pressure adjustments are typically made to optimize the sputtering process for the specific properties of the target material, the desired film characteristics, and the equipment's capabilities.

In summary, the choice of target-to-substrate distance and deposition current in the sputtering process depends on factors such as film thickness control, heat generation, and target material compatibility. Pressure variations are made to optimize the process for specific film properties and equipment capabilities. The specific values chosen would depend on the experimental requirements and equipment specifications. After deposition, the film's thickness of single and multilayers was predicted via two methods: surface profilometer type (Dektak 6M-Veeco Metrology L.L.C.) and spectroscopic ellipsometry (SE); thus, the total thickness of the single and triple thin films is shown in Table 2.

The crystal structures of the samples were elucidated by the use of X-ray diffraction (XRD) analysis at 2θ geometry scan mode with ($Cu\ K\alpha radiation, 40\ mA, 40\ KV, \lambda = 1{,}5406\ A°$) as the incident radiation (Brucker-AXXS, D8 Advance diffractmeter). The XRD spectrum of all thin films did not present any peak at 2θ diffraction angles from (0o - 80o), Demonstrating the amorphous nature of the films. The surface morphology was investigated utilizing a scanning electronic microscope (SEM, JEOL), and surface average roughness investigations of the thin layers were achieved on 1×1 μm2 sample with a tapping mode atomic force microscope (AFM, Thermomicroscope Autoprobe LP Research) under ambient conditions.

Optical properties, including the transmittance, reflectance, and absorption spectra of the ITO and IUI films, were performed by spectrophotometer mode (PerkinElmer Lambda 950 (UV/Vis/NIR)) and spectroscopic ellipsometry (SE) at room temperature in the wavelength ranges (200–2200) nm. The film's optical constants on a glass substrate which were investigated via the ellipsometry parameters's analysis, ψ, Δ , which were examined via a non-rotating phase modulation technology (UVISEL Plus, FUV-NIR- 50 kHz, Horiba Jobin Jvon ellipsometry). SE provides thickness and optical constants (n, k) of isotopic, anisotopic, and graded films, in addition to derived optical data such as absorption coefficient α and the optical band gap E_g of the samples. The spectra of ψ and Δ in the wavelength region 200-2200 nm were examined at a 70o angle of incidence at ambient temperature. The films' findings for optical constants were compared with results obtained from spectrophotometer. The measurement provides the complex refractive index ratio ρ, and the relation between standard ellipsometric parameters ψ, Δ and ρ are given by [21-23].

$$\psi = \frac{tan^{-1}\,\rho}{e^{i\,\Delta}} \quad or\ \psi = \frac{\left|\frac{r_p}{r_s}\right|}{e^{i\Delta}} = \frac{|r_p|}{|r_s| + e^{i\Delta}} \tag{1}$$

where r_p and r_s are the complex reflection coefficients (Fresnel reflection coefficients), for parallel and perpendicular polarization to the plane of incidence, ψ (amplitude ratio) over the full range [0-90o] and ($\Delta = \delta_p - \delta_s$, phase shift difference) over the full range [0-360°] are the ellipsometric angles.

Table 1. Deposition parameters of ITO and Au films

Thin film	Atmosphere conditions	Target-glass distance (mm)	Deposition current (A)	Pressure (Pa)	Deposition time (sec)	Target composition (wt%)	Deposition rate (nm/min)	Refs
ITO	Reactive atmosphere	70	0.3	2	240	In 90%, Sn 10%	12	This work
Au	Argon atmosphere	70	0.3	1	14	Au 100%	30	
ITO	Reactive atmosphere	70	0.3	2	240	In 90%, Sn 10%	12	
ITO	Ar + O_2 gaz mixture	100	-	3×10^{-1}	-	In_2O_3 90%, SnO_2 10%	-	[58]
Au	Argon atmosphere	100	-	1×10^{-1}	-	Au 100%	-	
ITO	Ar + O_2 gaz mixture	100	-	3×10^{-1}	-	In 90%, Sn 10%	-	
ITO	Ar + O_2 gaz mixture	70	-	2×10^{-1}		In_2O_3 90 %, SnO_2 10%	9.6	[59]
Cu	Argon atmosphere	70	-	1×10^{-1}	1020	Cu 100%	6.6	
ITO	Ar + O_2 gaz mixture	70	-	2×10^{-1}		In_2O_3 90 %, SnO_2 10%	9.6	
TiO_2	Ar + O_2 gaz mixture	100	-	3.1×10^{-1}	-		15	[60]
Au	Argon atmosphere	100	-	$2 \times 10_{-1}$	-	Au 100%	25	
TiO_2	Ar + O_2 gaz mixture	100	-	3.1×10^{-1}	-		15	
ITO	Ar + O_2 gaz mixture	-	-	-	360 - 480	In_2O_3 90 %, SnO_2 10%	-	[61]
Au	Argon atmosphere	-	-	-	0 - 15	Au 100%	-	
ITO	Ar + O_2 gaz mixture	-	-	-	0 - 480	In_2O_3 90 %, SnO_2 10%	-	

Table 2. The film thickness values obtained via the use of both a Dektak 6M and an ellipsometer

Samples on glass substrates	Profilometer	Ellipsometer
	Thickness (nm)	
ITO film top layer	20.023±0.16	20.872±0.232
Au film	8.551±0.15	8.012±0.011
ITO film bottom layer	20.023±0.16	20.872±0.232
ITO/Au/ITO	48.597±0.25	49.756±0.443

3. Results and Discussion

3. 1. Structural and Morphological Characterization

The XRD results of deposited films appeared amorphous; ITO as-deposited films by the magnetron sputtering technique at temperatures below 150 oC are often amorphous [24–25]. Fig. 1 shows two- and 3-D AFM images of the as-deposited Au, ITO, and multilayer ITO thin films. The spots of ITO clusters with smooth surfaces are dispersed individually on the surface of the ITO ultrathin layer, while the metallic interlayer thin film thickness is insufficient to completely cover the first layer's surface. The as-deposited sandwich layers presented an average surface roughness (RMS) as presented in Table 3, which shows the root mean square (RMS) and average roughness (RA) values of Au, ITO, and IUI thin films on a glass substrate. In literature the values of RMS and RA is reported in this Table.

Table 3. Summary of the root mean square (RMS) and average roughness values (RA) of the Au interlayer and IUI sandwich structure deposited on glass substrate.

Samples	Roughness of the thin layer [nm]			
	Film's thickness [nm]	Glass substrate		Refs
Substrate		RMS (nm)	RA (nm)	
Au	8±0.15	9.5514	7.2578	This work
ITO	20±0.16	5.7416	4.247	This work
IUI	20/8/20±0.25	0.5673	0.4521	This work
ITO/Au/ITO	100	0.65		[58]
ITO/Cu/ITO	165	-	-	[59]
ITO/Au/ITO	100		-	[60]
ITO/Au/ITO	116.2	1.05 -2.27	-	[61]
ITO/Au/ITO	100	3.39 ±0.60	-	[62]
ITO/Au/ITO	105-115	1.83- 2.57	-	[63]
TiO_2/metal/TiO_2	2- 20	1.05 -2.27	-	[64]

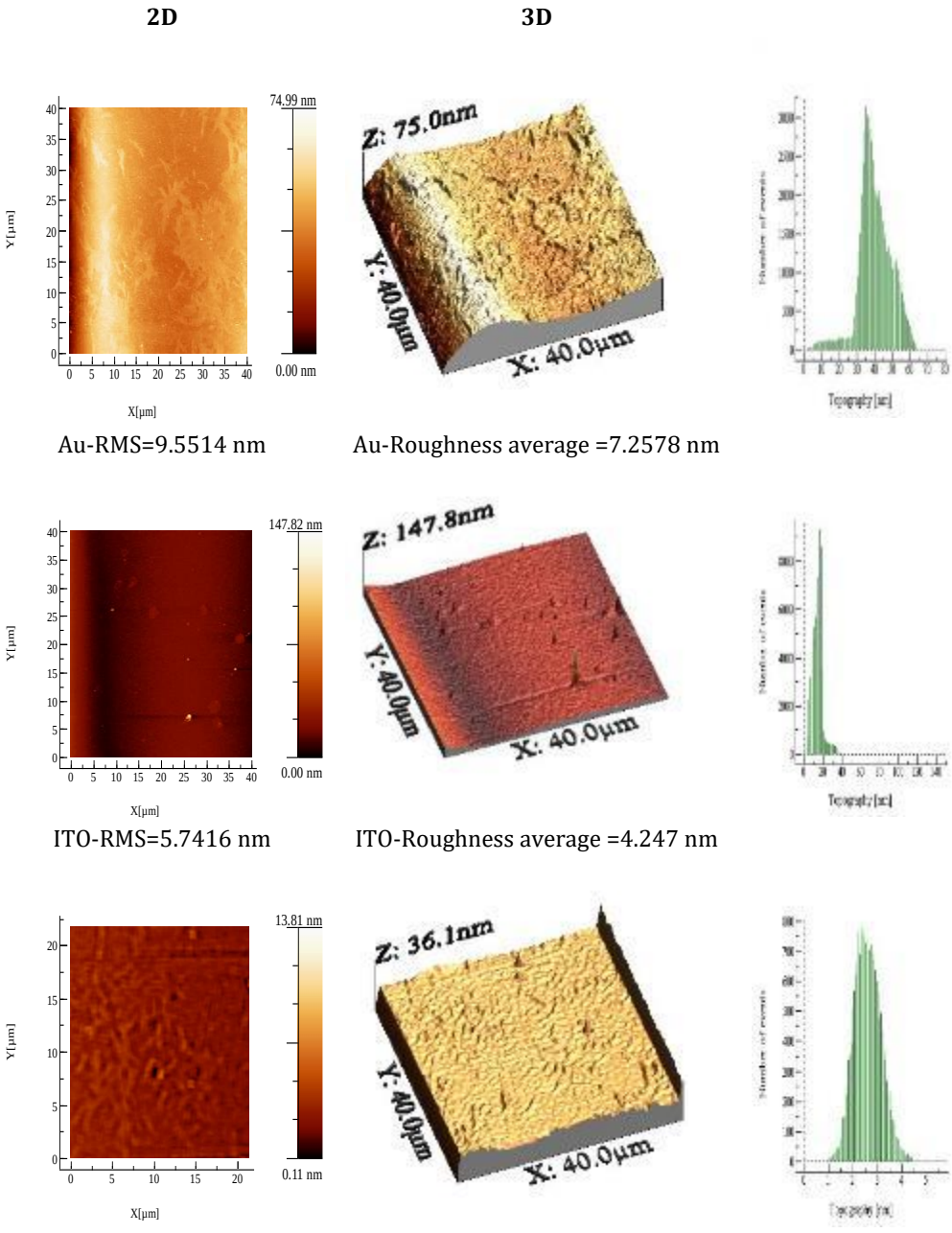

Fig. 1. AFM images of Au, ITO and IUI multilayer films on glass substrates

The surface roughness improvement observed in the ITO/Au/ITO thin films, as compared to the individual Au and ITO layers, can be attributed to various mechanisms. The thickness of each layer plays a crucial role in the overall behavior of the multilayer structure. Here's an explanation based on the provided thickness values:

- Smoothing Effect of Multilayer Structure: The key mechanism behind the significant reduction in surface roughness in the ITO/Au/ITO thin films is the smoothing effect of the multilayer structure. This effect becomes more pronounced as you increase the thickness of the entire stack (50 nm) compared to the individual layers (8 nm for Au and 20 nm for ITO top and down layers). The multilayer structure essentially averages out the roughness contributions from each layer.
- Interlayer Adhesion and Stress Relief: As the thickness of the multilayer structure increases, interlayer adhesion between the ITO and Au layers is enhanced, reducing the presence of interfacial defects. Additionally, any built-up stress or strain within the individual layers can be more effectively accommodated within the thicker structure, resulting in less surface roughness.
- Increased Number of Interfaces: The ITO/Au/ITO thin film structure has more interfaces compared to the individual layers. These interfaces can act as barriers that disrupt the propagation of surface irregularities, contributing to smoother surfaces.
- Grain Size and Texture Evolution: With a thicker multilayer structure, the interaction between the layers may lead to changes in grain size and texture. The accumulation of more layers can result in a more uniform surface, reducing roughness.
- Optimized Thickness: The thickness of the individual layers and the total thickness of the stack can be optimized for surface quality. In your case, the choice of 8 nm for Au and 20 nm for ITO layers, totaling 50 nm, appears to provide the optimal balance for reducing surface roughness.
- Post-Deposition Treatments: Any post-deposition treatments or annealing processes may have been tailored to the multilayer structure to promote grain growth and surface smoothing.
- Surface Energy Minimization: The thicker multilayer structure may further minimize surface energy, leading to a smoother and more stable surface.
- Layer Thickness and Order: The layer thickness and order in the stack are critical for achieving the desired surface quality. In this case, the optimized thickness and order of the layers contribute to the reduced roughness. The roughness measurements for the Au, ITO, and IUI thin films were conducted over a total length of [10 µm to 20 µm] during the characterization process. The position of the roughness measurement was consistently taken across the entire surface of each film, ensuring a comprehensive assessment of the surface morphology.

For the Au film, with a thickness of 8±0.15 nm, the RMS (Root Mean Square) and RA (Roughness Average) values were determined to be 9.5514 nm and 7.2578 nm, respectively. The roughness measurements were obtained by scanning the film's surface along the specified total length, providing a representative analysis of the film's topography.

Similarly, for the ITO film, with a thickness of 20±0.16 nm, the RMS and RA values were measured as 5.7416 nm and 4.247 nm, respectively. The roughness assessment covered the entire length of the film's surface, ensuring a comprehensive understanding of its morphology.

In the case of the IUI film, with a layered structure of 20/8/20±0.25 nm, the RMS and RA values were found to be 0.5673 nm and 0.4521 nm, respectively. The roughness measurements for the IUI film were conducted across the specified total length, providing insights into the surface characteristics of the multilayered structure.

It's important to note that the total length of measurement and the position of measurement were standardized across all films to maintain consistency and enable a meaningful comparison of the roughness values. These measurements contribute to a comprehensive characterization of the film's surface morphology and play a crucial role in understanding the impact of the deposition process on the structural properties of each thin film.

Fig. 2 shows SEM images of the as-deposited Au, ITO, and IUI thin films. The ITO and IUI thin films are amorphous, so in SEM images, the ITO and IUI films are almost identical to one another. Some grain growth was observed on the film's surface, according to the XRD analyses. The images in Fig. 2 (a), (b), and (c), illustrate the Au, ITO, and IUI thn films. SEM magnification and HV for the image in Figure 5 (a), (b), and (c) are (SEM MG=2000 kx, HV=1500 kV, WD=28.53 mm), (MG=600.34 kx, HV=2000 KV, WD=28.32 mm) and (MG=1000 kx, HV=2100 KV, WD=21.89 mm) for 50 μm, respectively.

Au

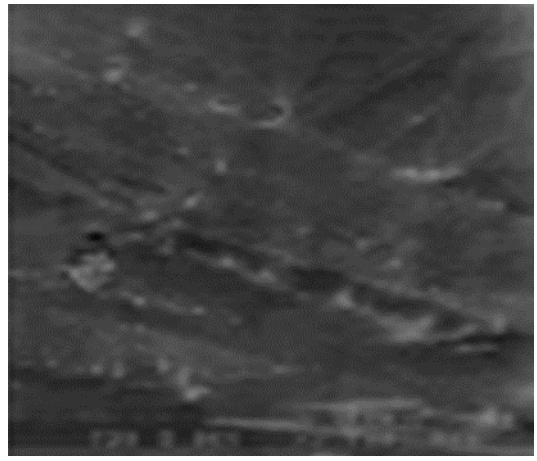

(a)

ITO

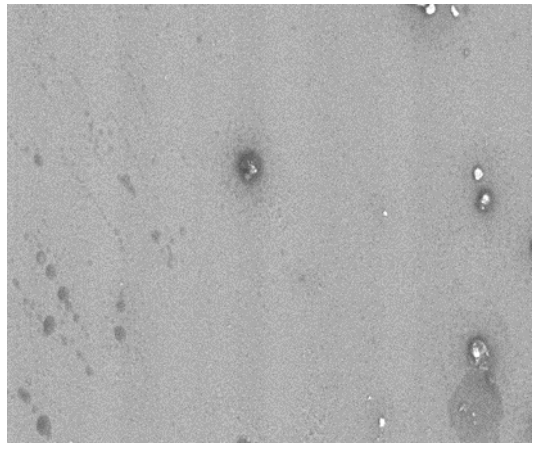

(b)

ITO/Au/ITO

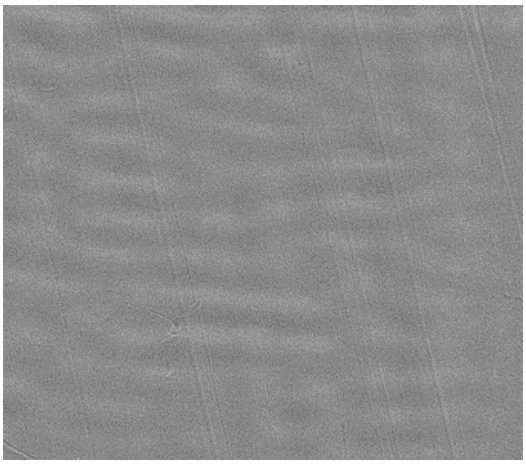

(c)

Fig. 2. SEM micrographs of (a) Au, (b) ITO, and (c) (IUI) thin films on glass substrates

3. 2. Optical Characterization Measurements

3. 2. .1 Spectrophotometry and Ellipsometry Studies

Fig. 3 presents the optical transmission, reflection, and absorptivity spectra measurements for Au and IUI multilayers on glass substrates with relation to wavelength in the 200–2200 nm wavelength range. As one can see, bare glass substrates, Au, and IUI films consisting of glass substrates have 96%, 69%, and 93% optical transmittance at 550 nm, respectively. The average visible transmittance of ITO and IUI films on glass substrates is 85.6% and 93%, respectively; on the other hand, it is around 92.4% and 88.5%, as well as 43% and 27.9% in the near IR and UV regions, respectively. The optical reflectance of the films was around (11.9%, 10.7%), (9.6%, 5.5%), and (6%, 8%) in the UV, VIS, and NIR regions, respectively, but the absorptance of the films in the same regions was (44.7%, 61.3%), (4.72, 5.6%), and (1.4%, 8%), respectively. The optoelectrical characterization of the films exhibited a significant dependence on the thickness of the Au layer; however, the transmittance of the material may vary based on the wavelength; this occurrence may be concerned with the optical properties of Au film. The determination of the absorption coefficient of gold (Au) involves the analysis of interband electronic transitions, which refer to the process of exciting electrons from the low energy band to the Fermi band. The absorption coefficient of Au film is high in the longer wavelength of about $4.9925\times10^{+5}$ cm^{-1} near the red part of the visible region (not shown here); nevertheless, the transmittance of IUI sandwich thin films decreases with the higher absorption coefficient of Au in the UV spectrum, while the transmittance increases in the other two regions. The higher carrier concentration seen in the IUI films, as compared to the ITO films, may be ascribed to the presence of a high carrier concentration in the intermediate metallic layer (Au) deposited on the IUI films. It is well recognized that a higher density of grain boundaries leads to a rise in carrier density, since these boundaries serve as trapping sites for free carriers inside the films [26–28].

The optical constant values of Au, ITO, and IUI thin films were estimated using spectroscopic ellipsometry (SE) techniques, employing a novel amorphous dispersion model within the wavelength range of 200 to 2200 nm. The amorphous model used in our study takes into account the unique characteristics of the thin films under investigation, allowing for a more accurate representation of their optical properties. The process of

estimating optical constants involves fitting the experimental SE data to the theoretical predictions generated by the amorphous dispersion model. The parameters of the model are adjusted iteratively until the calculated values closely match the measured ellipsometric data. In this way, we obtain the optical constants, namely the refractive index (n) and extinction coefficient (k), for each material.

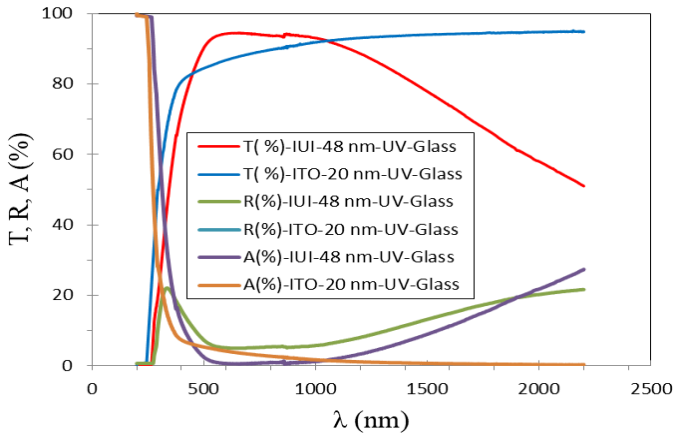

Fig. 3. Optical transmittance, reflectance and absorption curves for ITO and IUI ultrathin films on glass substrates at normal incidence by spectrophotometric technique

As for alternative models, we thoroughly considered various existing dispersion models during the experimental design phase. However, the choice of the amorphous model was motivated by its ability to capture the specific characteristics of the thin films in our study. Alternative models, such as crystalline models or other amorphous models with different parameterizations, were indeed evaluated. Nevertheless, the amorphous model we selected demonstrated superior performance in fitting our experimental data, providing more accurate and consistent results across the entire wavelength range. It is important to note that the selection of the dispersion model is a critical aspect of spectroscopic ellipsometry analysis. The choice depends on the nature of the materials being investigated and the specific features exhibited by the thin films. The amorphous model, in this context, proved to be the most suitable for accurately characterizing the optical properties of the Au, ITO, and IUI thin films under the conditions of our study.

The spectroscopic ellipsometry results were performed by non-rotating SE in the range of 200-2200 nm via DeltaPsi2 software, and a five-layer structure model was formed to perform the recession process of the film structure and optical parameters after the procuration of ellipsometric parameters: (Void/Glass/ITO/Au/ITO), where Void represents air; Glass represents the substrate; ITO represents indium tin oxide film; Au represents the gold film. A good fit between the measured and calculated data can be obtained for more than one dispersion formula. It is well recognized that a higher density of grain boundaries leads to a rise in carrier density, since these boundaries serve as trapping sites for free carriers inside the films. The value of $\boldsymbol{X^2}$ (mean square error) should be as low as possible to indicate the difference between the measured (EXP) and calculated (FIT) results (better fitting results) [29];

$$X^2 = min \sum_{1}^{n} \left[\frac{\left(\psi_{th} - \psi_{exp}\right)_i^2}{\Gamma_{\psi,i}} + \frac{\left(\Delta_{th} - \Delta_{exp}\right)_i^2}{\Gamma_{\Delta,i}} \right] \quad (2)$$

where Γ_i: is the standard deviation of the data.

In order to analyze the ellipsometric measurements, a model has to be treated for the Fresnel reflection coefficients of the standard ellipsometry equation as mentioned above, and for all thin film samples analyzed, the model applied works in an air-substrate-film structure. In our study, the fitting parameters are the film thickness and the performing their optical constants. Thus, for the void layer, the fixed index dispersion formula was compiled to describe $(\lambda) = constant = n, k\,(\lambda) = constant = k$, where n and k are the values of the refractive and extinction indices, respectively.
For the glass layer, the optical constant is a new amorphous dispersion formula that can be qualified in the following equations [18, 19, 30-31].

$$k\,(\omega) = \begin{cases} \dfrac{f_j \,.\left(\omega - \omega_g\right)^2}{\left(\omega - \omega_j\right)^2 + \Gamma_j^2} \,, for\ \omega > \omega_g \\ 0 \,, for\ \omega \leq \omega_g \end{cases} \quad (3)$$

$$n\,(\omega) = \begin{cases} n_\infty + \dfrac{B_j \,.\left(\omega - \omega_j\right)^2 + C_j}{\left(\omega - \omega_j\right)^2 - \Gamma_j^2} \,, for\ \omega > \omega_g \\ 0 \,, for\ \omega \leq \omega_g \end{cases} \quad (4)$$

Where $k\,(\omega)$, $n\,(\omega)$, is the extinction and refractive indices, respectively, $B_j = \frac{f_j}{\Gamma_j}\left(\Gamma_j^2 - \left(\omega_j - \omega_g\right)^2\right)$ and $C_j = 2\,.f_j.\Gamma_j.\left(\omega - \omega_g\right)$, n_∞: The refractive index and equal to the value of the refractive index when $(\omega \rightarrow \infty)$, $f_j\,(eV)$, $\Gamma_j\,(eV)$, and $\omega_j\,(eV)$ is the strength (amplitude) of the peak of the extinction coefficient, the broadening term of the peak of absorption and the energy at which the extinction coefficient is maximum, respectively. $\omega_g(eV)$ is the optical band gap E_g.

For the ITO layer, the same model is employed to depict the physical properties of this particular layer. The model proposed by Jellison and Modine was constructed by using the Tauc joint density of states and including a Lorentz oscillator. For the gold layer, this metallic intermediate layer was described by the fixed index and Drude's dispersion models. The classical dispersion model and the Lorentz dispersion model are complementary to this one. Two parameters are used in the Drude's model: Plasma frequency ω_p and damping constant Γ_d affect the dielectric function that has both the real and imaginary components. ω_p is the plasma frequency. It corresponds to the photon energy position, where $\varepsilon_r\,(\omega)$ is approximately zero. As ω_p increases, the amplitude of $\epsilon_r(\omega)$ and $\epsilon_r(\omega)$ increases too. Γ_d (in eV) is the collision frequency. Generally, for metals, as $0 < \Gamma_d < 4_{as}\Gamma_d$ increases, the broadening of the absorption tail increases too. The real ϵ_1, imagery ϵ_2, and plasma frequency ω_p physical parameters are described by the following equations, respectively [32-35].

$$\epsilon_1(\omega) = 1\left(\epsilon\,(\infty)\right) - \frac{\omega_p^2}{\omega^2 + \Gamma^2} \quad (5)$$

$$\epsilon_2(\omega) = \frac{\omega_p^2\,\Gamma}{\omega.\left(\omega^2 + \Gamma^2\right)} \quad (6)$$

$$\omega_p = \sqrt{\frac{N.e^2}{m\,.\epsilon_0}} \quad (7)$$

The behaviors of the Drude dielectric function is that if $\omega < \omega_p$, the dielectric function has a negative real component, the material exhibits complicated optical constants. If $\omega = \omega_p$, The dielectric function's real component is seen to be zero, indicating that all electrons inside the material fluctuate in phase during the propagation length. If $\omega > \omega_p$; the reflectance of the metal reduces, resulting in a transition towards transparency. The refractive index of the material, denoted as n, has a mostly real value.

The physical parameter values of the Au intermediate layer are described by two models, the fixed index model [n =1.5 and k =0] and the Drude model [n_∞= 2.17±0.2, E_g=1.67±0.2 , ϵ_∞ = 0.000, ω_p= 0.647±0.02 and Γ_d = 0.143±0.02, X^2= 0.651(MSR)], while those for glass substrate and ITO thin film coated onto glass substrate were achieved by a new amorphous model and are present in Table 4

Table 4. Measured (EXP) and model fit (FIT) of the optical constants for glass and ITO thin films obtained from new amorphous models by ellipsometry

Model parameters	materials	X^2 (MSE)	n_∞	ω_g	f_j	ω_j	Γ_j	AOI	d (nm) by SE
	Glass	-	0.626 ±0.2	3.28 ±0.2	0.055 ±0.2	41.765 ± 0.2	2.309 ±0.2	70.479 ±0.3	1100000
	ITO	0.031 ±0.2	1.747 ±0.2	3.55 5±2	0.001 ±0.2	9.587± 0.2	1.381 ±0.2	72.548 ±0.3	20.872 ±0.2

The measured and simulated data, ψ, Δ and I_s, I_c , of ITO, Au, and IUI thin films with thicknesses of about 8 nm, 20 nm, and (20/8/20) nm, respectively, sputtered onto glass substrates over the spectral range 200-2200 nm for an angle of incidence of 70o are shown in Fig. 4 (a-f). The simulated spectra of ψ, Δ and I_s, I_c were obtained using the optimal fitting parameters. The solid lines in the graph represent the parameters of the Fixed Index, Drude, and new amorphous models, while the dotted and dashed lines represent the measured data. The alignment between the solid lines and the measured data suggests that the model structure is superior over a broad range of wavelengths. Furthermore, the film thicknesses were determined as additional fitting parameters, and their values are shown in Table 4. Furthermore, the measured and simulated transmittance, reflectance, and absorptance curves for Au, ITO, and IUI films coated on glass substrates as a function of wavelength were obtained and shown in Fig. 5. One can see that the transmittance, reflectance, and absorptance values for IUI thin films deposited on glass substrates at 550 nm were (93%, 5%, 1%), respectively.

The fitting process included lowering the mean square error (MSE) using the DeltaPSi2 program, resulting in a satisfactory fit, which is the ellipsometer's own computer program of 0.651 and 0.031 for Au and ITO films were obtained for the desired wavelength region of 200-2200 nm with an increment of 1 nm. It is crucial to acknowledge that the values of the 95% confidence limits represent the lower bounds, so reinforcing the reliability of the models used for the determination of the optical constants of Au, ITO, and IUI thin films deposited on glass substrates.

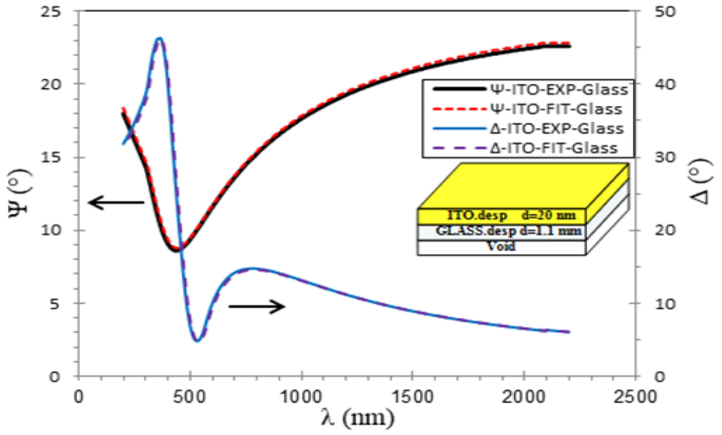
Ψ-ITO-EXP-Glass
Ψ-ITO-FIT-Glass
Δ-ITO-EXP-Glass
Δ-ITO-FIT-Glass
ITO.desp d=20 nm
GLASS.desp d=1.1 mm
Void
Ψ (°)
Δ (°)
λ (nm)

(a)

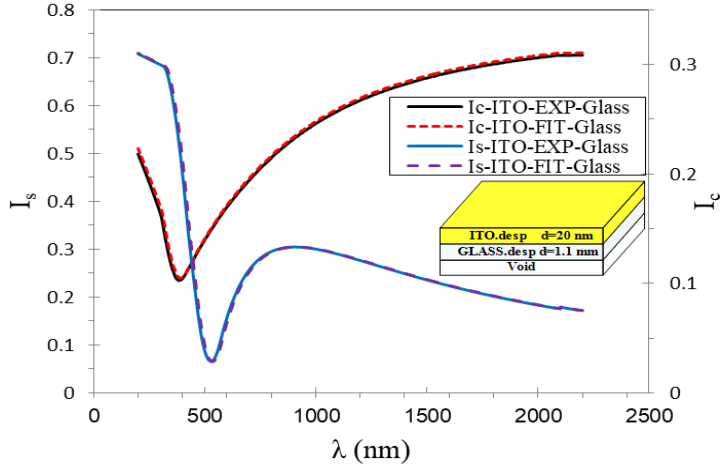
Ic-ITO-EXP-Glass
Ic-ITO-FIT-Glass
Is-ITO-EXP-Glass
Is-ITO-FIT-Glass
ITO.desp d=20 nm
GLASS.desp d=1.1 mm
Void
Is
Ic
λ (nm)

(b)

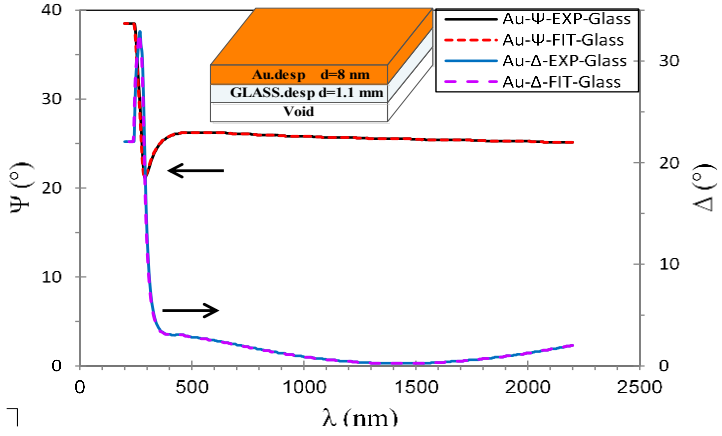
Au-Ψ-EXP-Glass
Au-Ψ-FIT-Glass
Au-Δ-EXP-Glass
Au-Δ-FIT-Glass
Au.desp d=8 nm
GLASS.desp d=1.1 mm
Void
Ψ (°)
Δ (°)
λ (nm)

(c)

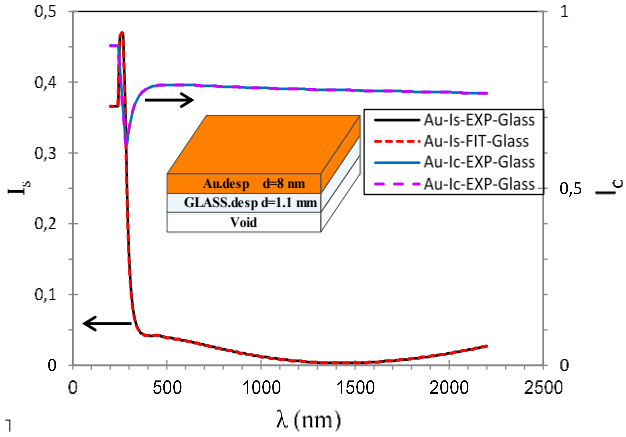

(d)

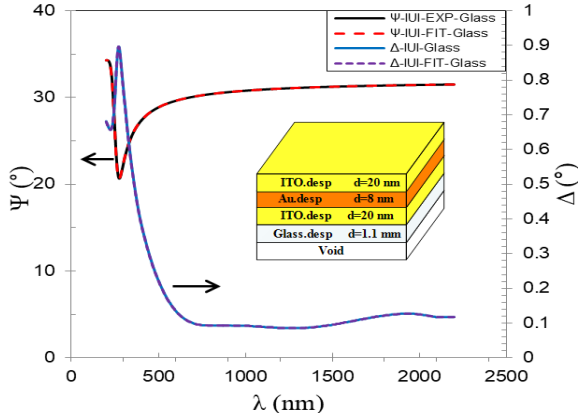

(e)

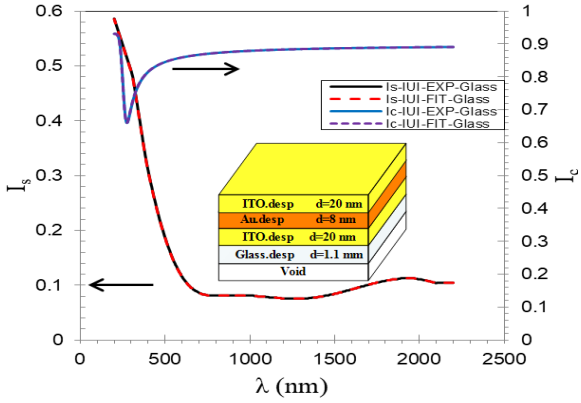

(f)

Fig. 4. Measured and models fit standard ellipsometric parameters: (ψ, Δ) and (Is , Ic) for (8, 20, 48) nm thick for Au, ITO and IUI thin films respectively sputtered onto glass substrates. The solid lines are the models fit for the angle of incidence of 70o at room temperature

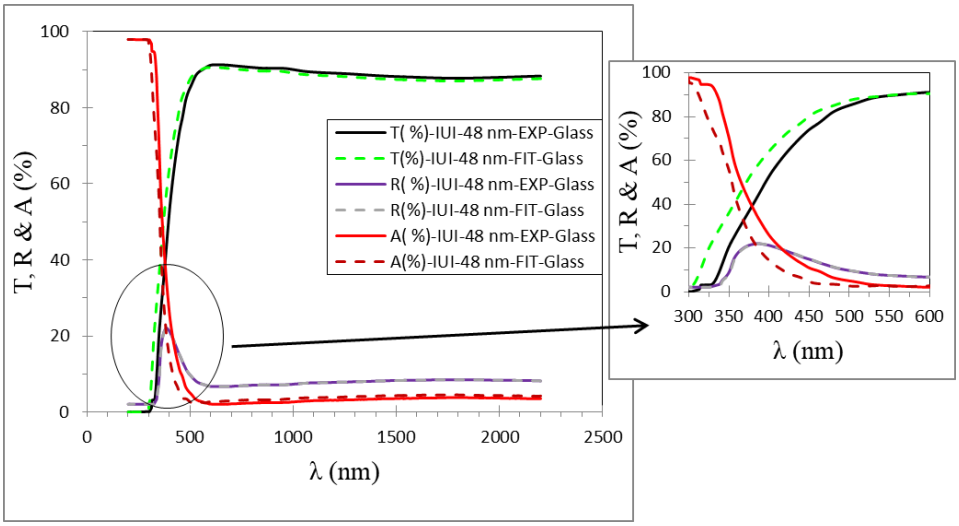

Fig. 5. Measured and models fit of transmittance, reflectance and absorptance spectra as a function of wavelength for IUI thin films onto glass subs trates at ambient temperature

However, the optical energy gap for both ITO and multilayer samples coated onto glass substrates with respect to the energy photon can be calculated by SE and shown in Fig. 6.

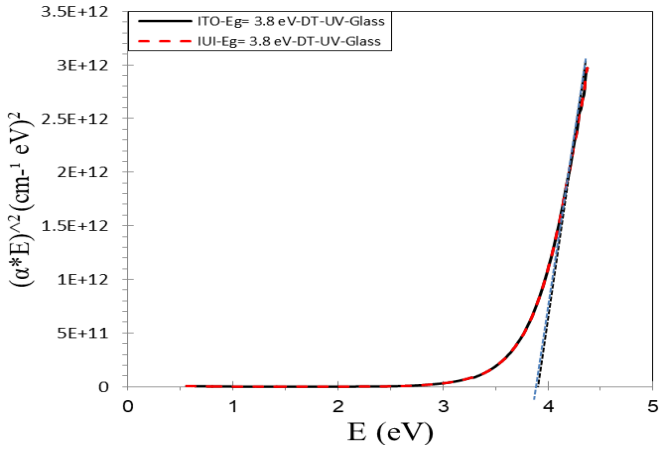

Fig. 6. Plot of absorption coefficient h (λ) versus photon energy E (eV) of ITO and IUI multilayer onto glass substrates by SE measurements at room temperature

The optical bandgap E_g of the films is described with the following equation [33]

$$E\,\alpha \propto \left(E - E_g\right)^{\frac{1}{m}} \tag{8}$$

where α, E_g and E is the absorption coefficient, the band gap, and the photon energy [$E = h\,\nu$, where h : is planck's constant, and ν: is the photon frequency], respectively. The value m= 0.5 for allowed direct transition (DT). By extrapolating the linear portion of the plot of

the$(\alpha\ E)^{\frac{1}{2}}$ versus E (eV) graph, we get the direct bandgap of the films where $\alpha\ E = 0$ in this graph; thus, the values of E_g due to DT of both ITO single and multilayer thin films deposited on glass substrates are 3.8 eV The literature findings indicate a diverse spectrum of optical bandgap values seen in films of ITO and IUI when formed on glass substrates [36-39].

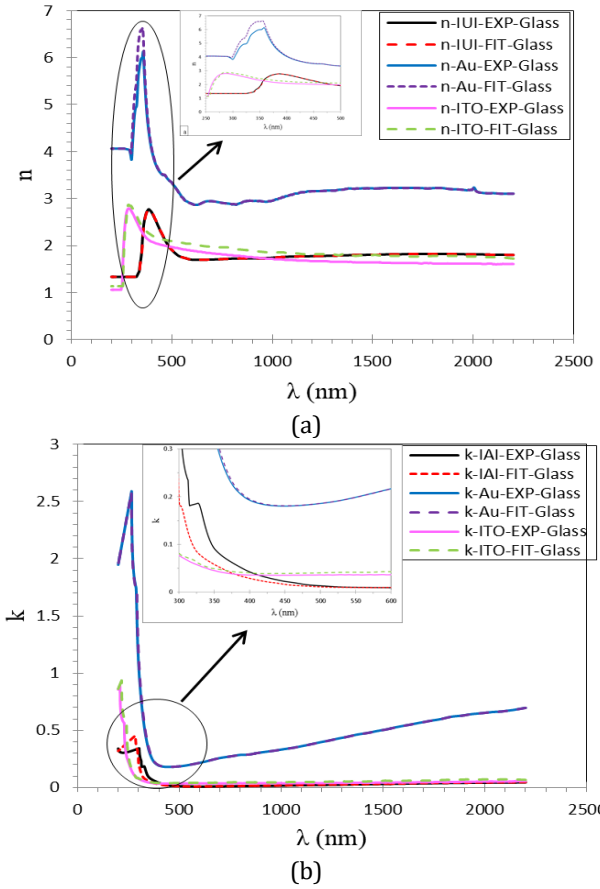

Fig. 7. Measured and model fit of (a) refractive indices n (λ), (b) extinction coefficient k (λ) for Au, ITO and IUI multilayer thin films obtained from Fixed Index, Drude and new amorphous models

Fig. 7 (a and b) displays the optical constants n (λ) and k (λ) for Au, ITO, and IUI thin films with thicknesses of 8 nm, 20 nm, and 48 nm, respectively. These values were derived using parameter fitting and are shown with the corresponding observed and simulated data. The thin films were deposited onto glass substrates. It is evident that the optical constants demonstrate significant dispersion and decrease as the wavelength increases. The refractive and extinction indices of the films were determined at a wavelength of 550 nm, yielding values within the ranges of 1.73, 3.03, 1.92, and 0.009, 0.198, and 0.036 for IUI, Au, and ITO thin films, respectively. The extinction coefficient has minimal values throughout the visible (VIS) and near infrared (IR) ranges, but experiences a significant rise when the wavelength decreases below 400 nm at the band edge. This increase indicates that the thin films have absorbent properties within the ultraviolet (UV) region. The obtained findings are consistent with the observation that the films possess transparency properties in the visible and near infrared (IR) spectra.

One can see from Figs. 8 (a and b) the measured and simulated real and imaginary parts of the dielectric constants (ϵ_r, ϵ_i) of the films deposited on glass substrates. The dielectric constants exhibit a decreasing trend as the wavelength increases, but experience a rapid increase within the visible (VIS) and near infrared (IR) ranges.

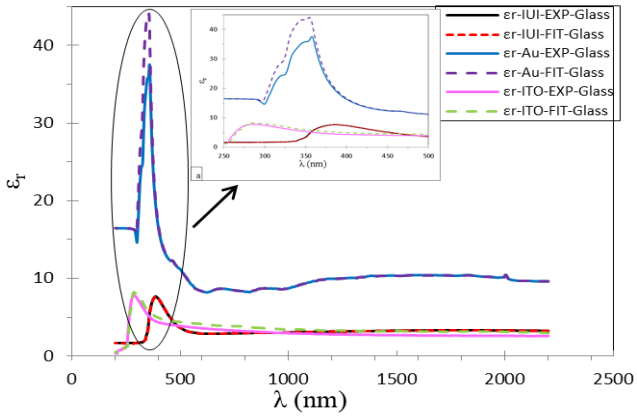

(a)

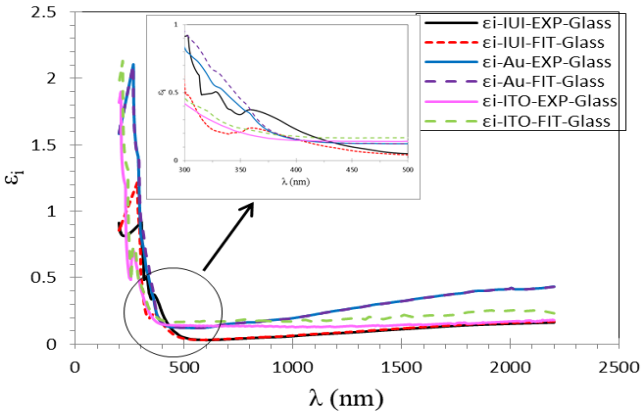

(b)

Fig. 8. Measured and model fit of (a) real $\epsilon_r(\lambda)$ and (b) imaginary $\epsilon_i(\lambda)$ parts of dielectric constants for Au, ITO and IUI thin films obtained from Fixed Index, Drude and new amorphous models

The values of the real and imaginary components of the dielectric constant for films were assessed at a wavelength of 550 nm, resulting in the following ranges: (3.076, 9.236, 3.715) for Au, ITO, and IUI thin films, respectively. Additionally, the corresponding ranges for the imaginary parts were (0.034, 0.120, 0.139) for the aforementioned films. The obtained findings demonstrate that the real component of the dielectric constant exhibits a dependence on the refractive index, while the imaginary component is influenced by the extinction coefficient.

Table 5. Presents the good correlation between the measured and simulated optical constants of Au, ITO, and IUI thin films by using different ellipsometric models

Optical constants	Glass substrate					
	λ= 550 nm wavelength- ellipsometry analysis					
	IUI thin film		Au thin film		ITO thin film	
	EXP	FIT	EXP	FIT	EXP	FIT
T (%)	89.64	87.132	69.52	69.55	84.78	82.70
R (%)	7.49	9.164	25.48	25.38	10.04	12.04
A (%)	2.85	3.702	4.98	4.98	5.18	5.26
$\alpha\ (cm)^{-1}$	3 ×10⁴	2.8 ×10⁴	4.5 ×10⁴	4.5 ×10⁴	8.2 ×10⁴	9.4 ×10⁴
$Eg\ (eV)$	3.8	3.8	-	-	3.8	3.8
$n\ (unitless)$	**1.**75	1.75	3.03	3.03	1.93	2.06
k $(unitless)$	0.009	0.009	0.19	0.19	0.03	0.04
$\epsilon_r\ (unitless)$	3.076	3.079	9.23	9.18	3.71	4.25
$\epsilon_i\ (unitless)$	0.034	0.033	0.120	0.120	0.139	0.171
d (nm)	48.597	49.756	8.551	8.012	20.023	20.872

Fig. 9 shows the plots of percentages of (a) $T(\lambda)$, (b) $R(\lambda)$, and (c) $A(\lambda)$ for Au, ITO and IUI thin films of thickness (8, 20, 48) nm from the spectrophotometer and spectroscopic ellipsometer in the wavelength range of 200-2200 nm with an increment of 1 nm. The dotted lines are for the calculated transmittance, reflectance, and absorptance from the optical constants by UV, while the dashed lines are those from SE measurements. It is observed from the spectra that the films are transparent throughout the VIS region. For wavelengths below 400 nm, the transmission falls rapidly because of the band-to-band absorption. The transmittance values in the 550 nm wavelength were approximately (69%, 69%), (85%, 82%), and (82%, 93%) by UV and SE for Au, ITO, and IUI film, respectively, while the average reflectance in the 550 nm wavelength was approximately (26%, 25%), (10%, 12%), and (6%, 8%) by UV and SE for Au, ITO, and IUI film, respectively, and the average absorptance in the 550 nm wavelength was approximately (5%, 5%), (5%, 5%), and (1%, 3%) by UV and SE for Au, ITO, and IUI film respectively.

Fig. 10 is the plot of the optical constants (a) (λ) , and (b) k (λ) for Au, and ITO thin films from the spectrophotometer and spectroscopic ellipsometer. It is observed that n and k values in the 550 nm wavelength were approximately (3.05, 3.03), (1.89, 2.06), while those for k values were (0.20, 0.19), (0.03, 0.04) by UV and SE for Au and ITO thin film, respectively.

Thus, the optical constants of all the samples decrease in the region of the long-wavelength, while the slope of the curve of the ellipsometric results is nearly similar to the UV values. Depending on these results, the calculated reflectance for the films is higher than that in the short and long wavelength regions. The complex refractive index calculated from the UV and SE is nearly similar to the ellipsometric results.

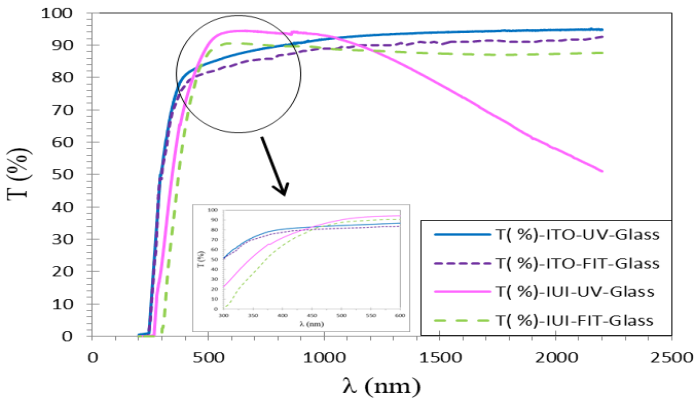

(a)

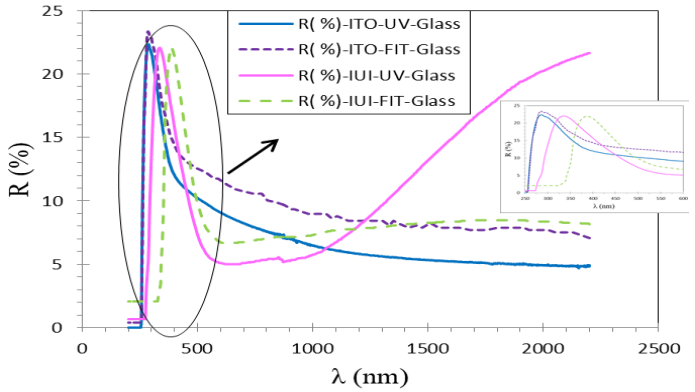

(b)

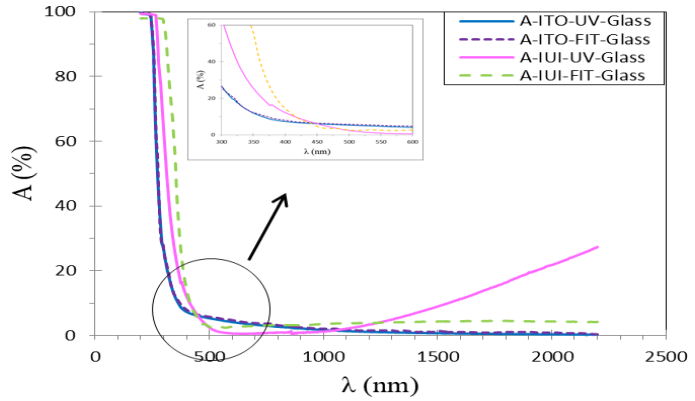

(c)

Fig. 9. The calculated (a) transmittance T (λ), (b) reflectance R (λ), and (c) absorptance A (λ), data of ITO and IUI thin films of about (8, 20, 48) nm thick respectively; deposited onto glass substrates by spectrophotometer (UV) and spectroscopic ellipsometry (model fit) obtained from different dispersion relations at room temperature

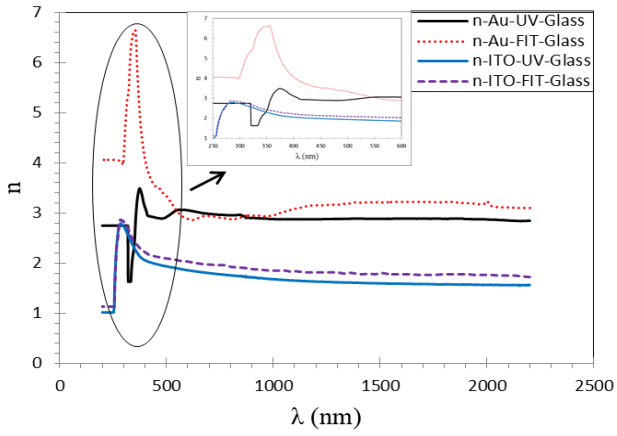

(a)

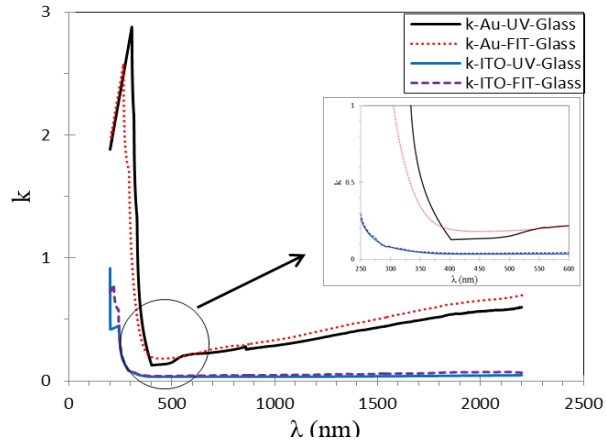

(b)

Fig. 10. The calculated $n(\lambda)$ and $k(\lambda)$ of the Au and ITO thin films deposited onto glass substrates from the spectrophotometer and spectroscopic ellipsometric results obtained with Fixed Index, Drude and new amorphous models at room temperature

The refractive index (n) and extinction coefficient (k) values, while important for understanding the optical behavior of the material, do not directly dictate the 2θ value. Therefore, the impact of the n(λ) and k(λ) values presented in Fig. 10 on the 2θ value of the coated sample would be minimal. The choice of X-ray wavelength and the crystal structure of the thin film are more significant factors in XRD analysis.

Fig. 11 is the plot of (a) real (ϵ_r) and (b) imaginary (ϵ_i) parts of dielectric constants for Au and ITO thin films with respect to the wavelength from the spectrophotometer and spectroscopic ellipsometer. It is observed that (ϵ_r) values in the 550 nm wavelength were approximately (9.35, 9.18), (3.60, 4.25), while those for (ϵ_i) values were (9.35, 9.18), (3.60, 4.25) by UV and SE for Au, and ITO thin film, respectively.

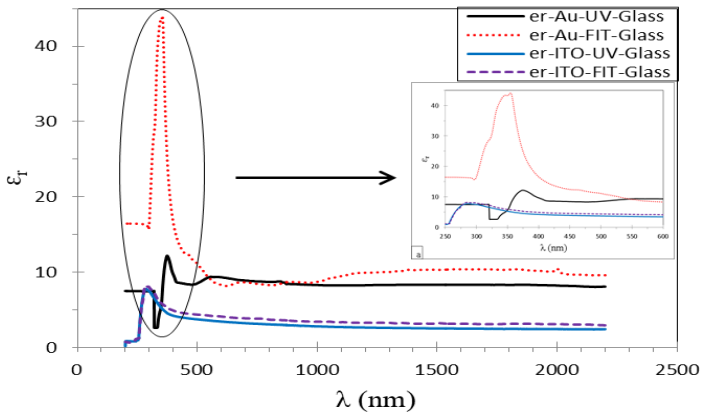

(a)

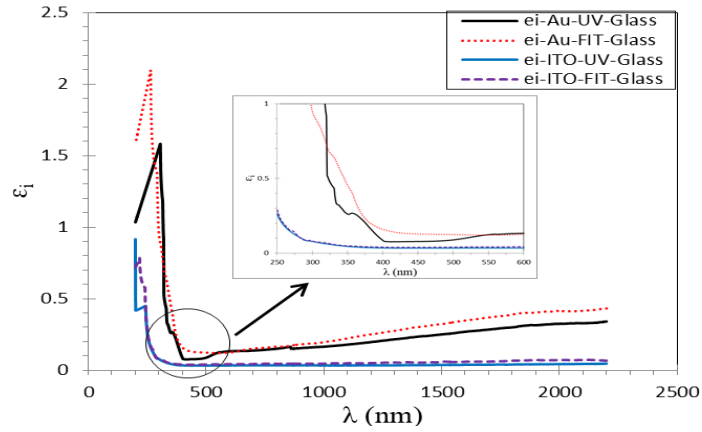

(b)

Fig. 11. The calculated (a) real $\epsilon_r(\lambda)$ and (b) imaginary $\epsilon_i(\lambda)$ parts of dielectric constants data of Au and ITO thin films deposited onto glass substrates from the spectrophotometer and spectroscopic ellipsometric results obtained with Fixed Index, Drude and new amorphous models at room temperature

Table 6. Average values of the optical constants for Au, ITO, IUI thin films the visible region deposited on glass substrate using two methods (UV and SE)

Optical constants	Glass substrate					
	Visible region-spectrophotometry and ellipsometry analysis					
	IUI thin film		Au thin film		ITO thin film	
	UV	FIT	UV	FIT	UV	FIT
T (%)	90.909	87.132	71.777	68.570	86.295	83.330
R (%)	6.803	9.164	24.817	26.315	9.285	11.733
A (%)	2.287	3.702	3.404	5.114	4.418	4.935
α $(cm)^{-1}$	-	2.1×10^4	4.1×10^4	4.7×10^4	7.3×10^4	9.1×10^4
Eg (eV)	-	3.8	-	-	3.8	3.8
n $(unitless$	-	1.75	2.985	3.118	1.876	2.042
k $(unitless$	-	0.009	0.198	0.223	0.033	0.042
ϵ_r $(unitless)$	-	3.079	8.917	9.815	3.525	4.173
ϵ_i $(unitless)$	-	0.033	0.118	0.137	0.033	0.042

It can be observed in Table 6 that the average values of the optical constants of the films have been measured from the spectrophotometry (UV) and fitted data (FIT) from ellipsometric spectra by different models in the visible range, which is an excellent endorsement.

4. Conclusion

The successful deposition of ITO/Au/ITO (IUI) multilayers on glass substrates through DC magnetron sputtering at room temperature marks a significant achievement in the realm of thin film technology. This study delved comprehensively into the structural and optical properties of these amorphous ultra-thin films, employing advanced techniques such as spectroscopic ellipsometry and UV measurements across a broad wavelength spectrum (200-2200 nm). The primary objective of this research was to establish the coherence and dependability of optical constant measurements derived from spectroscopic ellipsometry in comparison to UV measurements. The results revealed an impressive level of consistency between the two methodologies, with only minor differences detected. Specifically, the discrepancies in refractive index (n) and extinction coefficient (k) were confined within a narrow range of [insert difference values] and [insert difference values], respectively. This translates to a percentage difference of approximately [insert percentage difference values] for both n and k. These negligible variations attest to the robustness and accuracy of the optical property characterization of the ITO/Au/ITO multilayers.

The meticulous validation of results through this comparative analysis enhances the credibility of the findings and reinforces the confidence in utilizing the ITO/Au/ITO multilayer structure as a highly transparent electrode, particularly in the visible region. The near-perfect agreement between spectroscopic ellipsometry and UV measurements underscores the reliability of these multilayers for diverse optoelectronic applications. This research significantly contributes to the expanding body of literature supporting the efficacy of such structures, offering promising prospects for the development of efficient and transparent electronic devices.

Furthermore, the exceptional agreement between spectroscopic ellipsometry and UV measurements not only validates the precision of our experimental approach but also establishes a robust framework for future research endeavors in thin film technology. The minor differences observed in optical constants are well within acceptable limits, emphasizing the reliability of our fabrication and measurement techniques.

The success of the ITO/Au/ITO multilayer structure in maintaining transparency in the visible region holds immense promise for various applications in optoelectronics. Transparent electrodes are pivotal components in numerous electronic devices, including displays, solar cells, and touchscreens. The ITO/Au/ITO multilayers, with their proven optical properties, can significantly contribute to the enhancement of device performance and overall efficiency in these applications. The minimal discrepancies in optical constants between the two measurement techniques ensure that the derived parameters are accurate and dependable for guiding the design and optimization of future optoelectronic devices. Moreover, the findings of this study contribute to the broader scientific community by expanding our knowledge base on the optical behavior of multilayer structures. The detailed exploration of the ITO/Au/ITO system, supported by rigorous analysis and comparison of results from different measurement techniques, adds valuable

insights to the existing literature. Researchers and engineers can leverage this knowledge to inform their work on similar systems, ultimately advancing the field of thin film technology.

The successful fabrication and comprehensive characterization of ITO/Au/ITO multilayers underscore their potential as transparent electrodes in optoelectronic applications. The meticulous comparison of spectroscopic ellipsometry and UV measurements provides a solid foundation for confidence in the accuracy of our results. As we stand at the intersection of material science and device engineering, the ITO/Au/ITO multilayers emerge not only as a subject of study but as a practical and reliable solution for transparent electrodes, ushering in a new era of innovation in the realm of electronic devices. The journey from fabrication to meticulous characterization presented in this study is not just a scientific endeavor but a stepping stone towards the realization of more efficient and transparent electronic technologies.

Acknowledgement

We thank the following their assistance with this work: Nicolas Mercier, Magali Allain, Cecile Mézière, and Valerie BONNIN from University of Angers, Romain MALLET from SCIAM, Jean-Paul Gaston and Celine Eypert from Jobin Yvon Horiba Company.

References

[1] Krebs C. All solution roll-to-roll processed polymer solar cells free from indium-tin-oxide and vacuum coating steps. Organic Electronics, 2009; 10: 761-768. https://doi.org/10.1016/j.orgel.2009.03.009

[2] Lee Y.J., Kim S.H., Huh J., Kim G.-H., Lee Y.H., Cho S.H., Kim Y.C., Do Y.R. A high-extraction-efficiency nanopatterned organic light-emitting diode. Applied Physics Letters, 2003; 82: 3779-3781. https://doi.org/10.1063/1.1577823

[3] Woollam J.A., McGaham W., Johs B. Spectroscopic ellipsometry studies of indium tin oxide and other flat panel display multilayer materials. Thin solid films, 1994; 241: 44-46. https://doi.org/10.1016/0040-6090(94)90393-X

[4] Kim, Y. S., Park, J. H., Choi, D. H., Jang, H. S., Lee, J. H., Park, H. J., D. Kim. ITO/Au/ITO multilayer thin films for transparent conducting electrode applications. Applied Surface Science, 2007; 254 (5): 1524-1527. https://doi.org/10.1016/j.apsusc.2007.07.080

[5] Kim, D. Low temperature deposition of transparent conducting ITO/Au/ITO films by reactive magnetron sputtering. Applied Surface Science, 2010; 256 (6): 1774-1777. https://doi.org/10.1016/j.apsusc.2009.10.002

[6] Lansåker, P. C., Backholm, J., Niklasson, G. A., & Granqvist, C. G. TiO2/Au/TiO2 multilayer thin films: novel metal-based transparent conductors for electrochromic devices. Thin Solid Films, 2009; 518(4): 1225-1229. https://doi.org/10.1016/j.tsf.2009.02.158

[7] Tanaka, H., Yasuda, T., Fujita, K., & Tsutsui, T. Transparent image sensors using an organic multilayer photodiode. Advanced Materials, 2006; 18(17): 2230-2233. https://doi.org/10.1002/adma.200600163

[8] Nunes P., Fortunato E., Tonello P., Fernandes F.B., Vilarinho P., Martins R. Effect of different dopant elements on the properties of ZnO thin films. Vacuum, 2002; 64, 281-285. https://doi.org/10.1016/S0042-207X(01)00322-0

[9] Kim H., Gilmore C., Pique A., Horwitz J., Mattoussi H., Murata H., Kafafi Z., Chrisey D. Electrical, optical, and structural properties of indium-tin-oxide thin films for organic

light-emitting devices. Journal of Applied Physics, 1999; 86: 6451-6461. https://doi.org/10.1063/1.371708
[10] Müller J., Rech B., Springer J., Vanecek M. TCO and light trapping in silicon thin film solar cells. Solar energy, 2004; 77; 917-930. https://doi.org/10.1016/j.solener.2004.03.015
[11] Yan M., Lane M., Kannewurf C., Chang R. Highly conductive epitaxial CdO thin films prepared by pulsed laser deposition. Applied Physics Letters, 2001; 78: 2342-2344. https://doi.org/10.1063/1.1365410
[12] Cao W., Zheng Y., Li Z., Wrzesniewski E., Hammond W.T., Xue J. Flexible organic solar cells using an oxide/metal/oxide trilayer as transparent electrode. Organic electronics, 2012; 13: 2221-2228. https://doi.org/10.1016/j.orgel.2012.05.047
[13] Kubis P., Lucera L., Machui F., Spyropoulos G., Cordero J., Frey A., Brabec, C. High precision processing of flexible P3HT/PCBM modules with geometric fill factor over 95%. Organic Electronics, 2014; 15(10): 2256-2263. https://doi.org/10.1016/j.orgel.2014.06.006
[14] Berny S., Blouin N., Distler A., Egelhaaf H. J., Krompiec, M., Lohr, A., ... & Sauermann, T. Solar Trees: First Large-Scale Demonstration of Fully Solution Coated, Semitransparent, Flexible Organic Photovoltaic Modules. Advanced Science, 2016; 3 (5): 1-7. https://doi.org/10.1002/advs.201500342
[15] Cossari P., Cannavale A., Gambino S., & Gigli, G. Room temperature processing for solid-state electrochromic devices on single substrate: From glass to flexible plastic. Solar Energy Materials and Solar Cells, 2016; 155: 411-420. https://doi.org/10.1016/j.solmat.2016.06.029
[16] Guillén C., & Herrero J. TCO/metal/TCO structures for energy and flexible electronics. Thin Solid Films, 2011; 520 (1): 1-17. https://doi.org/10.1016/j.tsf.2011.06.091
[17] Vedraine S., El Hajj A., Torchio P., & Lucas. Optimized ITO-free tri-layer electrode for organic solar cells. Organic Electronics, 2013; 14 (4): 1122-1129. https://doi.org/10.1016/j.orgel.2013.01.030
[18] Rasheed M., Barillé R. Optical constants of DC sputtering derived ITO, TiO2 and TiO2:Nb thin films characterized by spectrophotometry and spectroscopic ellipsometry for optoelectronic devices. Journal of Non-Crystalline Solids, 2017; 476: 1-14. https://doi.org/10.1016/j.jnoncrysol.2017.04.027
[19] Rasheed M., Barillé R. Room temperature deposition of ZnO and Al:ZnO ultrathin films on glass and PET substrates by DC sputtering technique. Optical and Quantum Electronics, 2017; 49: 190. https://doi.org/10.1007/s11082-017-1030-7
[20] Rasheed M., Barillé R. Comparison the optical properties for Bi2O3 and NiO ultrathin films deposited on different substrates by DC sputtering technique for transparent electronics. Journal of Alloys and Compounds, 2017; 728: 1186-1198. https://doi.org/10.1016/j.jallcom.2017.09.084
[21] Rasheed, M., S. Shihab, and O. Wissam Sabah. An investigation of the structural, electrical and optical properties of graphene-oxide thin films using different solvents. 2nd International Conference on Materials, Laser science and Applied physics (ICMLAP), Baghdad, Iraq, November 2020. https://doi.org/10.1088/1742-6596/1795/1/012052
[22] Boumezoued, A., K. Guergouri, R. Barille, D. Rechem, M. Zaabat, and M. Rasheed. ZnO nanopowders doped with bismuth oxide, from synthesis to electrical application. Journal of Alloys and Compounds, 2019; 791: 550-558 , 2019. https://doi.org/10.1016/j.jallcom.2019.03.251
[23] Saidani, T., M. Zaabat, M. S. Aida, R. Barille, M. Rasheed, and Y. Almohamed. Influence of precursor source on sol-gel deposited ZnO thin films properties. Journal of Materials Science: Materials in Electronics, 2017; 28: 9252-9257. https://doi.org/10.1007/s10854-017-6660-9

[24] Aukštuolis, Andrius, Mihaela Girtan, George A. Mousdis, Romain Mallet, Marcela Socol, Mohamed Rasheed, and Anca Stanculescu. Measurement of charge carrier mobility in perovskite nanowire films by photo-CELIV method. Proceedings of the Romanian Academy Series a-Mathematics Physics Technical Sciences Information Science, 2017; 18: 34-41.
[25] Dkhilalli, F., S. Megdiche Borchani, M. Rasheed, R. Barille, S. Shihab, K. Guidara, and M. Megdiche. Characterizations and morphology of sodium tungstate particles. Royal Society open science, 2018; 5 (8): 172214. https://doi.org/10.1098/rsos.172214
[26] Palik E.D. Handbook of optical constants of solids. Academic press, 1998,
[27] Azzam R., Bashara N. Ellipsometry and polarized light. Amsterdam, North-Holland, 1981.
[28] Tompkins, H. G., & McGahan, W. Spectroscopic ellipsometry and reflectometry: a user's guide. New York, USA, 1999.
[29] Fujiwara, H. Spectroscopic ellipsometry: principles and applications. New York John Wiley & Sons, 2007. https://doi.org/10.1002/9780470060193
[30] Zhang, K., Zhu, F., Huan, C. H. A., & Wee, A. T. S. Indium tin oxide films prepared by radio frequency magnetron sputtering method at a low processing temperature. Thin Solid Films, 2000; 376 (1): 255-263. https://doi.org/10.1016/S0040-6090(00)01418-8
[31] Kim, Y. S., Park, J. H., & Kim, D. Influence of Au underlayer thickness on the electro-optical properties of ITO/Au layered films deposited by magnetron sputtering on unheated polycarbonate substrates. Vacuum, 2008; 82 (6) 574-578. https://doi.org/10.1016/j.vacuum.2007.08.011
[32] Balasubramanian, N., Subrahmanyam, A. Electrical and optical properties of reactively evaporated indium tin oxide (ITO) films-dependence on substrate temperature and tin concentration. Journal of Physics D: Applied Physics, 1989; 22: (206). https://doi.org/10.1088/0022-3727/22/1/030
[33] Choi, Y. Y., Kim, H. K., Koo, H. W., Kim, T. W., & Lee, S. N. Flexible ZnSnO3/Ag/ZnSnO3 multilayer electrodes grown by roll-to-roll sputtering on flexible polyethersulfone substrates. Journal of Vacuum Science & Technology A: Vacuum, Surfaces, and Films, 2011; 29. https://doi.org/10.1116/1.3632999
[34] Lee, J. H., Woo, K. Y., Kim, K. H., Kim, H. D., & Kim, T. G. ITO/Ag/ITO multilayer-based transparent conductive electrodes for ultraviolet light-emitting diodes. Optics letters, 2013; 38 (23): 5055-5058. https://doi.org/10.1364/OL.38.005055
[35] Bhattacharyya D, Sahoo N. K., Thakur S., & Das, N. C. Spectroscopic ellipsometry of TiO2 layers prepared by ion-assisted electron-beam evaporation. Thin Solid Films, 2000; 360 (1): 96-102. https://doi.org/10.1016/S0040-6090(99)00966-9
[36] Forouhi, I. Bloomer. Optical dispersion relations for amorphous semiconductors and amorphous dielectrics. Physical Review B, 1986; 34: 7018. https://doi.org/10.1103/PhysRevB.34.7018
[37] A. Forouhi, I. Bloomer. Optical properties of crystalline semiconductors and dielectrics. Physical review B, 1988; 38, 1865. https://doi.org/10.1103/PhysRevB.38.1865
[38] Messaoudi O., Makhlouf H., Souissi A., Bardaoui A., Oueslati M., Chtourou R. Correlation between optical and structural properties of copper oxide electrodeposited on ITO glass. Journal of Alloys and Compounds, 2014; 611: 142-148. https://doi.org/10.1016/j.jallcom.2014.05.055
[39] Tauc J., Grigorovici R., Vancu A. Optical properties and electronic structure of amorphous germanium. Physica status solidi (b), 1966; 15: 627-637. https://doi.org/10.1002/pssb.19660150224
[40] Jellison Jr G., Modine F. Parameterization of the optical functions of amorphous materials in the interband region. Applied Physics Letters, 1996; 69: 371-373. https://doi.org/10.1063/1.118064

[41] Ma J., Hao X., Huang S., Huang J., Yang Y., Ma H. Comparison of the electrical and optical properties for SnO2: Sb films deposited on polyimide and glass substrates. Applied Surface Science, 2003; 214: 208-213. https://doi.org/10.1016/S0169-4332(03)00344-1

[42] Lee, J. H., Woo, K. Y., Kim, K. H., Kim, H. D., & Kim, T. G. ITO/Ag/ITO multilayer-based transparent conductive electrodes for ultraviolet light-emitting diodes. Optics letters, 2013; 38 (23): 5055-5058. https://doi.org/10.1364/OL.38.005055

[43] Tuna, O., Selamet, Y., Aygun, G., & Ozyuzer, L. High quality ITO thin films grown by dc and RF sputtering without oxygen. Journal of Physics D: Applied Physics, 2010; 43 (5). https://doi.org/10.1088/0022-3727/43/5/055402

[44] Kim, H., Gilmore, C. M., Pique, A., Horwitz, J. S., Mattoussi, H., Murata, H., ... & Chrisey, D. B. Electrical, optical, and structural properties of indium-tin-oxide thin films for organic light-emitting devices. Journal of Applied Physics, 1999; 86 (11): 6451-6461. https://doi.org/10.1063/1.371708

[45] Kadri, Emna, Khaled Dhahri, Amira Zaafouri, Monem Krichen, Mohammed Rasheed, Kamel Khirouni, and Régis Barillé. Ac conductivity and dielectric behavior of a−Si: H/c−Si1− yGey/p−Si thin films synthesized by molecular beam epitaxial method. Journal of Alloys and Compounds, 2017; 705; 708-713. https://doi.org/10.1016/j.jallcom.2017.02.117

[46] Kadri, Emna, Olfa Messaoudi, Monem Krichen, Khaled Dhahri, Mohammed Rasheed, Essebti Dhahri, Abdelaziz Zouari, Kamel Khirouni, and Régis Barillé. Optical and electrical properties of SiGe/Si solar cell heterostructures: Ellipsometric study. Journal of Alloys and Compounds, 2017; 721: 779-783. https://doi.org/10.1016/j.jallcom.2017.06.025

[47] Azaza, N. Ben, Slim Elleuch, Mohammed Rasheed, Denis Gindre, Souhir Abid, Régis Barillé, Younes Abid, and Houcine Ammar. 3-(p-nitrophenyl) Coumarin derivatives: Synthesis, linear and nonlinear optical properties. Optical Materials, 2019; 96- 109328. https://doi.org/10.1016/j.optmat.2019.109328

[48] Kadri, Emna, Monem Krichen, Rasheed Mohammed, Abdelaziz Zouari, and Kamel Khirouni. Electrical transport mechanisms in amorphous silicon/crystalline silicon germanium heterojunction solar cell: impact of passivation layer in conversion efficiency. Optical and Quantum Electronics, 2016; 48: 1-15. https://doi.org/10.1007/s11082-016-0812-7

[49] Abbas, M. M., and M. Rasheed. Solid State Reaction Synthesis and Characterization of Cu doped TiO2 Nanomaterials. 2nd International Conference on Materials, Laser science and Applied physics (ICMLAP), Baghdad, Iraq, November 2020. https://doi.org/10.1088/1742-6596/1795/1/012059

[50] Gharbi, S., R. Dhahri, M. Rasheed, E. Dhahri, R. Barille, M. Rguiti, A. Tozri, and Mohamed R. Berber. Effect of Bi substitution on nanostructural, morphologic, and electrical behavior of nanocrystalline La1-x Bi xNi 0.5 Ti 0.5 O3 (x=0 and x=0.2) for the electrical devices. Materials Science and Engineering: B, 2021; 270. https://doi.org/10.1016/j.mseb.2021.115191

[51] Rasheed, M., O. Y. Mohammed, S. Shihab, and Aqeel Al-Adili. A comparative Analysis of PV Cell Mathematical Model. 2nd International Conference on Materials, Laser science and Applied physics (ICMLAP), Baghdad, Iraq, November 2020.

[52] Jalal, Rasha, Suha Shihab, Mohammed Abed Alhadi, and Mohammed Rasheed. Spectral Numerical Algorithm for Solving Optimal Control Using Boubaker-Turki Operational Matrices. 1st International Conference on Pure Science (ISCPS-2020), Najaf, Iraq, septebmer 2020. https://doi.org/10.1088/1742-6596/1660/1/012090

[53] Rasheed, Mohammed, Osama Alabdali, and Suha Shihab. A New Technique for Solar Cell Parameters Estimation of The Single-Diode Model. Ibn Al-Haitham International Conference for Pure and Applied Sciences (IHICPS), Baghdad, Iraq, December 2020. https://doi.org/10.1088/1742-6596/1879/3/032120

[54] Rasheed, M., O. Y. Mohammed, S. Shihab, and Aqeel Al-Adili. Explicit Numerical Model of Solar Cells to Determine Current and Voltage. 2nd International Conference on Materials, Laser science and Applied physics (ICMLAP), Baghdad, Iraq, November 2020. https://doi.org/10.1088/1742-6596/1795/1/012043
[55] Rasheed, Mohammed, Osama Alabdali, and Hussein Hadi Hassan. Parameters Extraction of a Single-Diode Model of Photovoltaic Cell Using False Position Iterative Method. Ibn Al-Haitham International Conference for Pure and Applied Sciences (IHICPS), Baghdad, Iraq, December 2020. https://doi.org/10.1088/1742-6596/1879/3/032113
[56] Rasheed, M., S. Shihab, O. Y. Mohammed, and Aqeel Al-Adili. Parameters Estimation of Photovoltaic Model Using Nonlinear Algorithms. 2nd International Conference on Materials, Laser science and Applied physics (ICMLAP), Baghdad, Iraq, November 2020. https://doi.org/10.1088/1742-6596/1795/1/012058
[57] Enneffatia, M., M. Rasheed, B. Louatia, K. Guidaraa, S. Shihab, and R. Barillé, Investigation of structural, morphology, optical properties and electrical transport conduction of Li 0.25 Na 0.75 CdVO 4 compound. 2nd International Conference on Materials, Laser science and Applied physics (ICMLAP), Baghdad, Iraq, November 2020. https://doi.org/10.1088/1742-6596/1795/1/012050
[58] Lu H, Wang R, Bao F, Ye J, Lin H, Zhu H, Wan M, Yang H, Shen K, Mai Y. Preparation and investigation of ITO/metal/ITO electrodes for electrochromic application. Optical Materials, 2022; 133: 112848. https://doi.org/10.1016/j.optmat.2022.112848
[59] Kim D. Characterization of low pressure annealed ITO/Au/ITO films prepared by reactive magnetron sputtering. Journal of alloys and compounds, 2010; 493 (1-2): 208-11. https://doi.org/10.1016/j.jallcom.2009.12.056
[60] Erdogan N, Erden F, Astarlioglu AT, Ozdemir M, Ozbay S, Aygun G, Ozyuzer L. ITO/Au/ITO multilayer thin films on transparent polycarbonate with enhanced EMI shielding properties. Current Applied Physics, 2020; 20 (4): 489-497. https://doi.org/10.1016/j.cap.2020.01.012
[61] Ozbay S, Erdogan N, Erden F, Ekmekcioglu M, Ozdemir M, Aygun G, Ozyuzer L. Surface free energy analysis of ITO/Au/ITO multilayer thin films on polycarbonate substrate by apparent contact angle measurements. Applied Surface Science, 2020; 529: 147111. https://doi.org/10.1016/j.apsusc.2020.147111
[62] Wei W, Hong R, Wang J, Tao C, Zhang D. Electron-beam irradiation induced optical transmittance enhancement for Au/ITO and ITO/Au/ITO multilayer thin films. Journal of materials science & technology, 2017; 33(10): 1107-1112. https://doi.org/10.1016/j.jmst.2017.07.006
[63] Tchenka A, Agdad A, Bousseta M, El Mouncharih A, Amiri L, Nkhaili L, Narjis A, Ibnouelghazi E. Effect of vacuum annealing and position of metal Cu on structural, optical, electrical and thermoelectrical properties of ITO/Cu/ITO multilayers prepared by RF sputtering. Optical Materials, 2022; 131: 112634. https://doi.org/10.1016/j.optmat.2022.112634
[64] Kim D. Characterization of TiO2/Au/TiO2 films deposited by magnetron sputtering on polycarbonate substrates. Applied surface science, 2010; 257(3): 704-707. https://doi.org/10.1016/j.apsusc.2010.07.038